Key Engineering Materials
ISSN: 1662-9795, Vol. 926, pp 2109-2118
doi:10.4028/p-1ydx9o

Submitted: 2021-12-08
Revised: 2022-01-28
Accepted: 2022-02-03
Online: 2022-07-22

Viscoplastic Self-Consistent (VPSC) Modeling for Predicting the Deformation Behavior of Commercial EN AW-7075-T651 Aluminum Alloy

Josef Domitner[1,a,*], Ricardo H. Buzolin[1,2,b], Samiksha Patil[1,3,c], Peter Auer[1,d], Nikolaus Papenberg[3,e], Evgeniya Kabliman[3,4,f], Zahra Silvayeh[1,g], Andreas Drexler[1,h], and Florian Grabner[3,i]

[1]Graz University of Technology (TUG), Institute of Materials Science, Joining and Forming, Research Group of Lightweight and Forming Technologies, Inffeldgasse 11/I, 8010 Graz, Austria

[2]Christian Doppler Laboratory (CDL) for Design of High-Performance Alloys by Thermomechanical Processing, Kopernikusgasse 24, 8010 Graz, Austria

[3]Austrian Institute of Technology (AIT), Light Metals Technologies Ranshofen (LKR), Lamprechtshausenerstraße 61, 5282 Ranshofen, Austria

[4]Technical University of Munich (TUM), Chair of Materials Engineering of Additive Manufacturing, Boltzmannstraße 15, 85748 Garching/Munich, Germany

[a]josef.domitner@tugraz.at, [b]ricardo.buzolin@tugraz.at, [c]samiksha.patil@student.tugraz.at, [d]p.auer@tugraz.at, [e]nikolaus.papenberg@ait.ac.at, [f]evgeniya.kabliman@tum.de, [g]zahra.silvayeh@tugraz.at, [h]andreas.drexler@tugraz.at, [i]florian.grabner@ait.ac.at

Keywords: metal forming, aluminum alloy, texture, crystallographic orientation, VPSC modeling

Abstract. Viscoplastic self-consistent (VPSC) modeling was used for investigating the deformation behavior of commercial EN AW-7075-T651 aluminum alloy at room temperature under quasi-static tension and compression (i) parallel, (ii) diagonal and (iii) transverse to the rolling direction. Textures of the as-received plate and of the samples after tensile and compression testing were determined using electron backscatter diffraction (EBSD). Euler angles and area fractions of the grains were used as input for calculating direction-dependent flow curves and pole figures of the deformed material. The coefficients of the integrated Voce strain hardening law were adjusted in order to fit the calculated flow curves to flow curves obtained from tensile and compression testing. Pole figures calculated with the VPSC modeling method were validated with pole figures obtained from EBSD analysis of deformed samples. VPSC modeling was successfully applied for predicting the general deformation behavior of EN AW-7075-T651 under both tension and compression. However, texture evolution during tensile testing was negligible, whereas notable texture evolution during compression testing occurred beyond a critical strain value.

Introduction

The crystallographic orientation of grains within polycrystalline materials, the so-called texture, is of major interest in forming processes, as it significantly influences the deformation behavior of the material and the mechanical properties of the final product [1-3]. Since detailed information about the anisotropy of texture is crucial for manufacturing high-quality products, different numerical methods describing the texture evolution and the associated properties during thermal or mechanical processing have been developed [4,5]. Especially viscoplastic self-consistent (VPSC) modeling has been established as reliable method for investigating texture evolution during plastic deformation [6,7]. It has been successfully employed for investigating different steels and non-iron alloys, including in particular aluminum alloys of the 1xxx [8], 2xxx [9-11], 5xxx [11-20], 6xxx [11,20-22] and 7xxx [11,22-24] series.

In the present work VPSC modeling was used for calculating the flow curves and the texture represented by the pole figures of commercial high-strength EN AW-7075-T651 aluminum alloy subjected to both quasi-static tension and compression at room temperature. Age-hardenable 7xxx aluminum alloys are important lightweight materials used in the aviation industry for producing aircraft structures. They combine favorable mechanical properties including high specific strength,

stiffness and toughness, as well as beneficial technological properties such as excellent processing, machining and welding performances [25].

Experiments

Material specification and sample preparation. The deformation behavior of a 20 mm-thick rolled plate of EN AW-7075-T651 (Al-5.5Zn-Mg-Cu) aluminum alloy at room temperature was studied under both quasi-static tension and compression. Table 1 contains the chemical composition of the alloy according to the supplier's specification. Three tensile samples and three compression samples were tested parallel (0°/RD), diagonal (45°/RD-TD) as well as transverse (90°/TD) to the rolling direction of the plate. The bone-shaped tensile samples with dimensions according to DIN 50125 type H were milled, whereas the comparatively small compression samples with dimensions of Ø 10 mm × 10 mm were wire-cut. In order to analyze the microstructure, for each load direction one as-received and one deformed sample were cut, cold-embedded into acrylic resin, ground using SiC paper and polished using silica oxide polishing suspension (OP-S).

Table 1: Chemical composition of EN AW-7075-T651 aluminum alloy (wt%)

Si	Mg	Cu	Zn	Fe	Cr	Mn	Ti	Al
0.17	2.6	1.5	5.9	0.24	0.19	0.04	0.04	bal.

Mechanical testing. Zwick/Roell Z100 uniaxial testing machines were used for both tensile and compression testing. Elongation of the samples was tactilely measured using a mechanical extensiometer, whereas compression of the samples was optically measured using a GOM ARAMIS 3D camera system. Tensile testing was performed according to OENORM EN ISO 6892-1 at constant strain rate of 6.7×10^{-3} s^{-1}. Compression testing was conducted at constant punch speed of 1 mm/min up to the maximum load of 100 kN, i.e., the average strain rate was approx. -1.7×10^{-3} s^{-1}. Teflon-based lubricant was used for reducing friction between the compressed cylindrical samples and the punches.

Microstructure analysis. A TESCAN Mira3 scanning electron microscope (SEM) and the APEX software package were used for electron backscattered diffraction (EBSD) measurements on the microstructures of as-received and deformed samples. The acceleration voltage was 30 kV and the spot size was 80 nm. Sample areas from 0.8 mm × 0.8 mm to 1.4 mm × 1.4 mm with step sizes of 0.7-1.2 µm were investigated. The OIM Analysis 8.6 software was used for analyzing the EBSD data and for exporting the Euler angles, which were required as input for VPSC modeling and for plotting the pole figures. The angle of 15° [26] was defined as transition between low-angle grain boundaries (LAGB) and high-angle grain boundaries (HAGB). The confidence index of the grains was standardized and the EBSD data was then cleaned via grain dilation, considering the minimum confidence index of 0.1 and the minimum grain size of 5 µm.

Simulation

Flow curves of EN AW-7075-T651 and the texture evolution of this aluminum alloy during tensile and compression deformation were calculated using the viscoplastic self-consistent (VPSC) code VPSC 7c developed by Lebensohn and Tomé [27]. A comprehensive description of the underlying model which considers both of the crystal plasticity mechanisms, slipping and twinning, is provided elsewhere [28]. The VPSC simulation performed in this work considers <111>{110} slip systems, but they neglect twinning of the grains.

The VPSC model describes a polycrystal as collection of crystallographic orientations (grains) with associated weights (volume fractions). Each of these statistically representative grains is regarded as ellipsoidal, viscoplastic inclusion embedded in and interacting with a viscoplastic homogeneous effective medium (HEM) which represents the polycrystal. Both, inclusion and HEM have fully anisotropic properties. A self-consistent approach applied to the weighted average of the

grains gives the macroscopic viscoplastic compliance, and the sum of the microscopic responses of all grains yields the macroscopic response of the polycrystal. For each grain at position vector **x** the deviatoric viscoplastic strain rate, $\dot{\boldsymbol{\varepsilon}}(\mathbf{x})$, is calculated using the symmetric Schmid tensor, $\mathbf{m}^s(\mathbf{x})$, and the local shear rate, $\dot{\gamma}^s$, acting on the slip system s of the grain [27,28]:

$$\dot{\boldsymbol{\varepsilon}}(\mathbf{x}) = \sum_s \dot{\gamma}^s(\mathbf{x})\mathbf{m}^s(\mathbf{x}) = \dot{\gamma}_0 \sum_s \mathbf{m}^s(\mathbf{x}) \left(\frac{\mathbf{m}^s(\mathbf{x}):\boldsymbol{\sigma}(\mathbf{x})}{\hat{\tau}^s}\right)^n \quad (1)$$

$$\mathbf{m}^s(\mathbf{x}) = \frac{1}{2}\left(\mathbf{b}^s(\mathbf{x}) \otimes \mathbf{n}^s(\mathbf{x}) + \mathbf{n}^s(\mathbf{x}) \otimes \mathbf{b}^s(\mathbf{x})\right) \quad (2)$$

$\mathbf{m}^s(\mathbf{x})$ is calculated based on the Burgers vector $\mathbf{b}^s(\mathbf{x})$ and on the normal vector $\mathbf{n}^s(\mathbf{x})$ which are both associated to the slip system s. $\boldsymbol{\sigma}(\mathbf{x})$ is the deviatoric stress acting on the grain, $\dot{\gamma}_0$ is the normalization factor and n is the rate sensitivity exponent. Activation of a slip system takes place once the shear stress reaches the threshold shear stress $\hat{\tau}^s$. For each grain the evolution of $\hat{\tau}^s$ with accumulated microscopic shear strain, Γ, is calculated using the Voce strain hardening law [27-29]:

$$\hat{\tau}^s(\Gamma) = \tau_0^s + (\tau_1^s + \theta_1^s\Gamma)\left(1 - \exp\left(-\Gamma\left|\frac{\theta_0^s}{\tau_1^s}\right|\right)\right) \quad (3)$$

The constitutive parameters τ_0^s, $(\tau_0^s + \tau_1^s)$, θ_0^s and θ_1^s are the initial critical resolved shear stress (CRSS), the back-extrapolated CRSS, the initial hardening rate and the asymptotic hardening rate, respectively. For the range of deformation speed used in this work the flow stress was assumed as independent from the strain rate, i.e., the simulation did not consider any strain rate sensitivity. The interaction between grains and HEM in terms of stress and strain rate was assumed to obey the tangent self-consistent approach [27,28]. Table 2 summarizes the VPSC modeling parameters used in the present work.

Table 2: VPSC modeling parameters

Parameter	Symbol	Value	Source
Initial CRSS	τ_0	180.0 MPa	based on flow curves determined within this work and similar to [11]
Back-extrapolated CRSS	$\tau_0 + \tau_1$	219.5 MPa	
Initial hardening rate	θ_0	395.0 MPa	
Asymptotic hardening rate	θ_1	48.5 MPa	
Grain major axis ratio	—	2.1826	based on EBSD measurements performed within this work
Grain intermediate axis ratio	—	2.1826	
Grain minor axis ratio	—	0.2000	
Elastic stiffness constants for f.c.c. aluminum	C_{11}	108.2 GPa	according to [30] and similar to [31]
	C_{12}	61.3 GPa	
	C_{44}	28.5 GPa	

In this work the crystallographic texture is represented by (001), (111) and (110) pole figures. These figures were calculated based on the Euler angles of the grains and plotted with the halfwidth of 10° and with the resolution of 1° using the standard method of the MTEX toolbox [32], which is available for the Matlab software package.

Results and Discussion

Texture of as-received material. Figure 1 characterizes the texture of the as-received material which was used as input for VPSC modeling. The axes at the front corner of the cubes indicate the grain orientation with respect to the rolling (RD), transversal (TD) and normal (ND) directions.

Thermomechanical production of the aluminum alloy plate caused considerable elongation of the grain morphology in RD, as shown by the inverse pole figure (IPF) cube in Figure 1 (a). The grain orientation spread (GOS) cube in Figure 1 (b) shows recrystallized grains with misorientation spread < 1° (blue). Small misorientation spread from 1°-10° (green, yellow, orange) indicates moderately deformed grains, whereas high misorientation spread > 10° (red) indicates heavily deformed grains. Black lines mark high-angle grain boundaries (HAGB). Figure 1 (c) shows three pole figures of the (001), (111) and (110) planes characterizing the typical texture of the as-received EN AW-7075-T651 aluminum alloy. Typical {110}<-112> brass texture with the texture index maximum of 4.4 was determined for the (110) plane. The axes next to the color bar indicate the crystal orientation with respect to the sample.

The diagrams shown in Figure 1 (d) and (e) confirm that the texture within the sample areas investigated is strongly anisotropic. Even though grain sizes and grain shapes are similar in RD and TD, they are quite different in ND. The peaks of the curves shown in the diagrams for RD and TD indicate that most of the grains have cross-section areas from approx. 200 µm^2 to 0.02 mm^2 and aspect ratios less than approx. 0.2, which confirms that the grains are strongly elongated in RD and TD. In contrast, most of the grains have large cross-section areas up to 0.2 mm^2 and comparatively high aspect ratios in ND. Therefore, the grains appear larger but less squeezed in ND than in RD and TD, which agrees well with the grain morphologies visualized in Figure 1 (a) and (b).

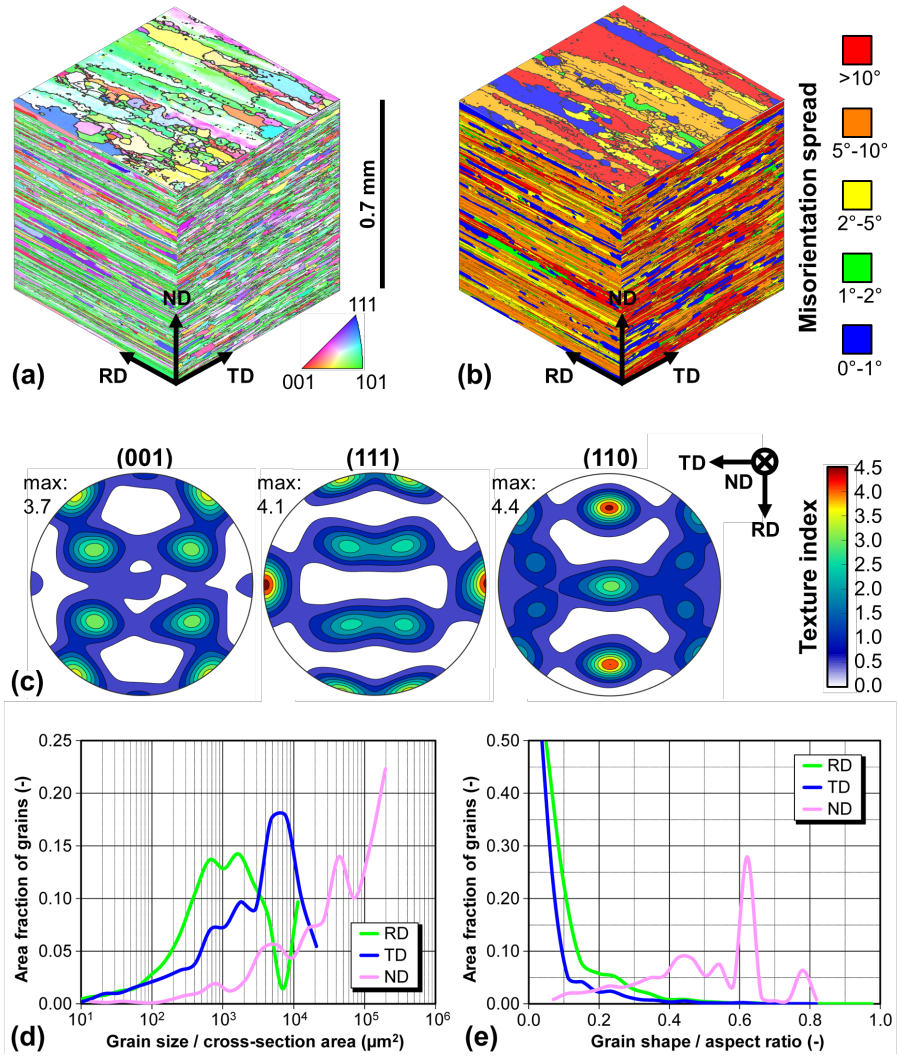

Figure 1: Microstructure characterization of the as-received material based on electron-backscattered diffraction (EBSD) measurements; (a) inverse pole figure (IPF) cube, (b) grain orientation spread (GOS) cube, (c) pole figures of (001), (111) and (110) planes, and area fraction of grains classified based on (d) the grain size and (e) the grain shape.

Flow curves. Figure 2 compares the flow curves (i.e., true stress vs. true strain) of EN AW-7075-T651 aluminum alloy for both (a) tension and (b) compression determined by mechanical testing (measurements, M) and VPSC modeling (simulation, S). The flow curves obtained in this work are within the range of flow curves (or true stress-strain curves) reported for the same alloy, heat treatment and load conditions in previous studies [33-35]. Maximum strain of $\varepsilon_t \approx 0.08$ and $\varepsilon_t \approx 0.22$ were achieved under tensile load and compression load, respectively, before necking or bulging of the samples started. The simulation overestimates strain hardening in each of the directions RD, RD-TD and TD under tension, even though the yield stress between measurements and simulation agrees. In contrast, the simulation can predict strain hardening under compression in both RD and TD quite well; however, strain hardening is different in RD-TD. Hence, the true stress in RD-TD was underestimated for $\varepsilon_t < 0.25$, but it was overestimated for $\varepsilon_t > 0.25$.

Despite the differences between the results of measurements and simulation, VPSC modeling can be considered as feasible method for predicting flow curves of EN AW-7075-T651 depending on the load condition (tension or compression) as well as on the direction of deformation. Particular differences between measurements and simulation could be attributed to (i) the intrinsic limitation of the utilized Voce law which only considers simple strain hardening behavior, or to (ii) the single-phase approach which considers aluminum grains, but neglects further phases. The investigated aluminum alloy typically contains additional particles aligned in RD that are virtually undeformable compared to the aluminum matrix [36,37].

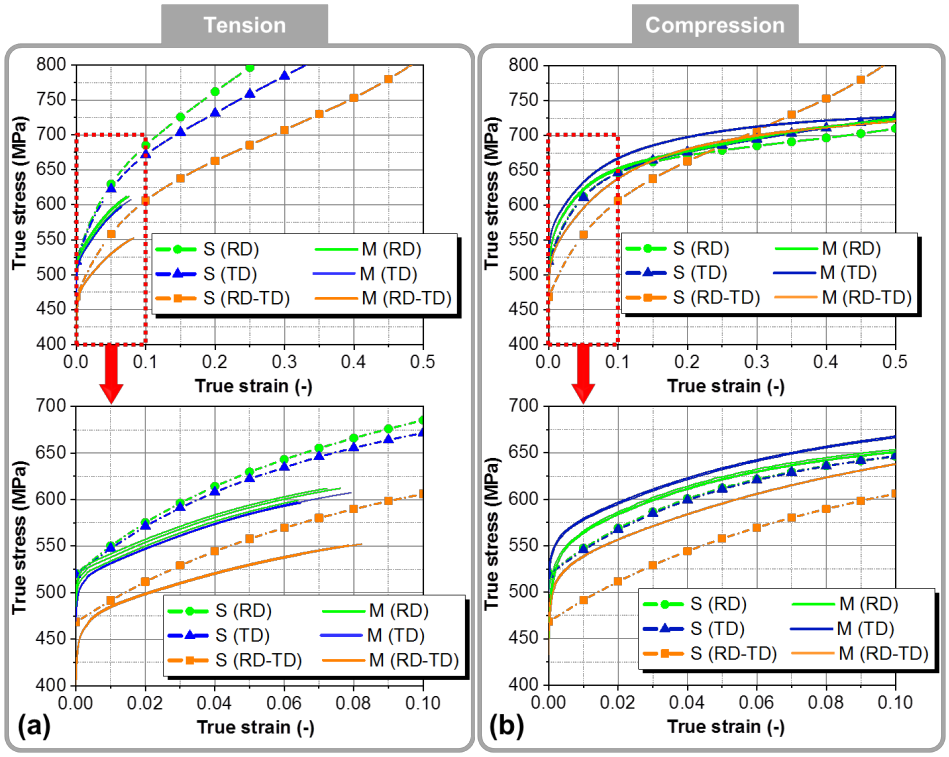

Figure 2: Flow curves of EN AW-7075-T651 for (a) tension and (b) compression determined by simulation (S) and measurements (M).

Texture evolution. Pole figures representing the texture evolution of EN AW-7075-T651 aluminum alloy under tension ($\varepsilon_t \approx 0.08$), Figure 3, and under compression ($\varepsilon_t \approx 0.6$), Figure 4, were calculated by means of VPSC modeling (a-c) and measured by means of EBSD (d-f) for each of the sample directions RD, RD-TD and TD. Figure 5 shows in detail the evolution of the pole figures during compression in RD-TD, which illustrates exemplarily the transformation of the brass texture of the as-received material into the 45°-rotated Goss texture of the deformed material. The axes at the top of each figure indicate the crystal orientation with respect to the sample.

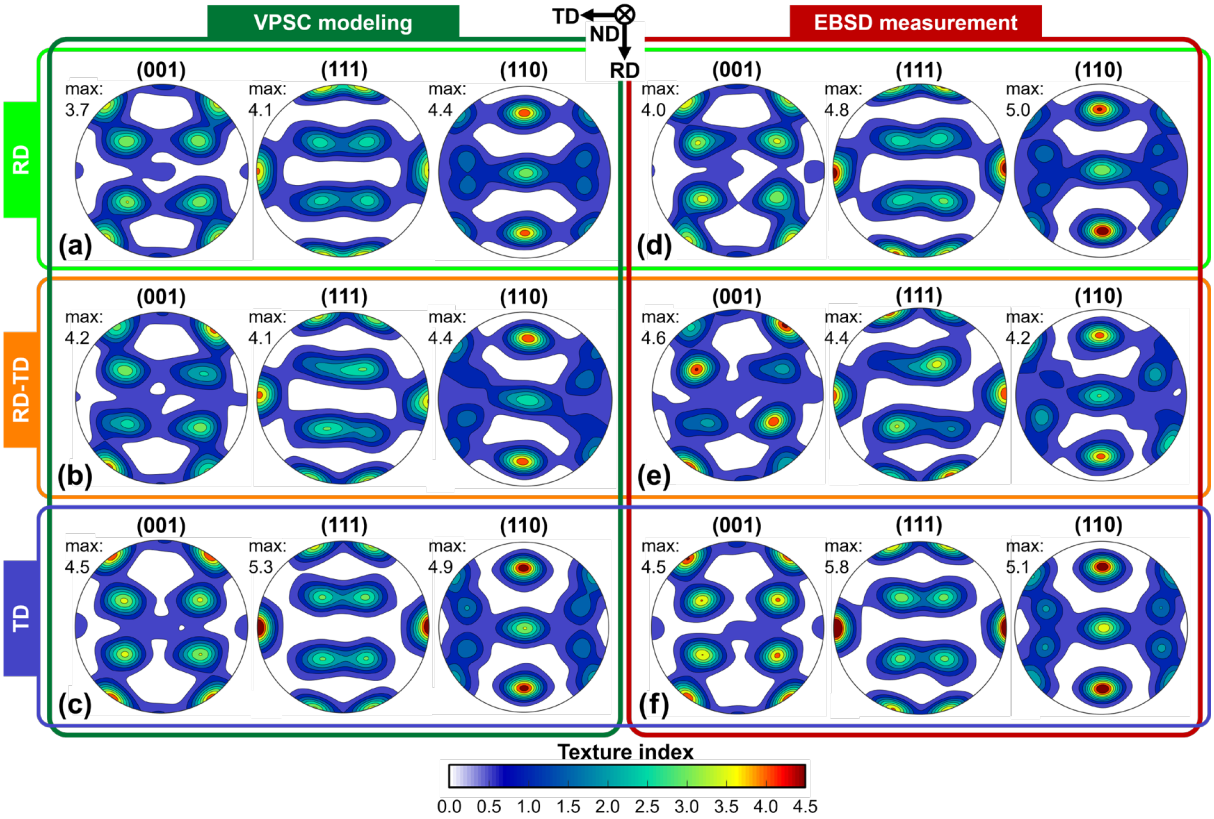

Figure 3: Pole figures of (001), (111) and (110) planes for tensile strain of approx. 0.08 obtained from (a-c) simulation and from (d-f) measurements in (a,d) RD, (b,e) RD-TD and (c,f) TD.

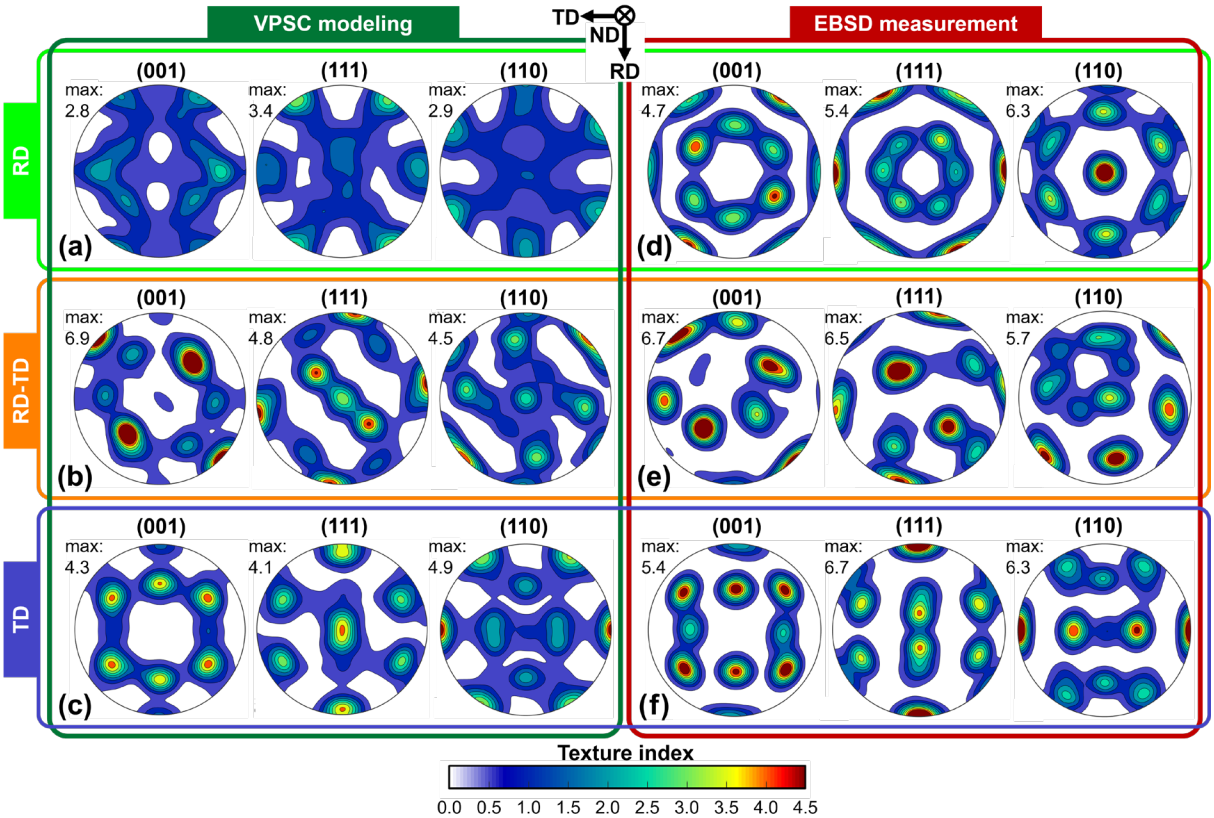

Figure 4: Pole figures of (001), (111) and (110) planes for compression strain of approx. 0.6 obtained from (a-c) simulation and from (d-f) measurements in (a,d) RD, (b,e) RD-TD and (c,f) TD.

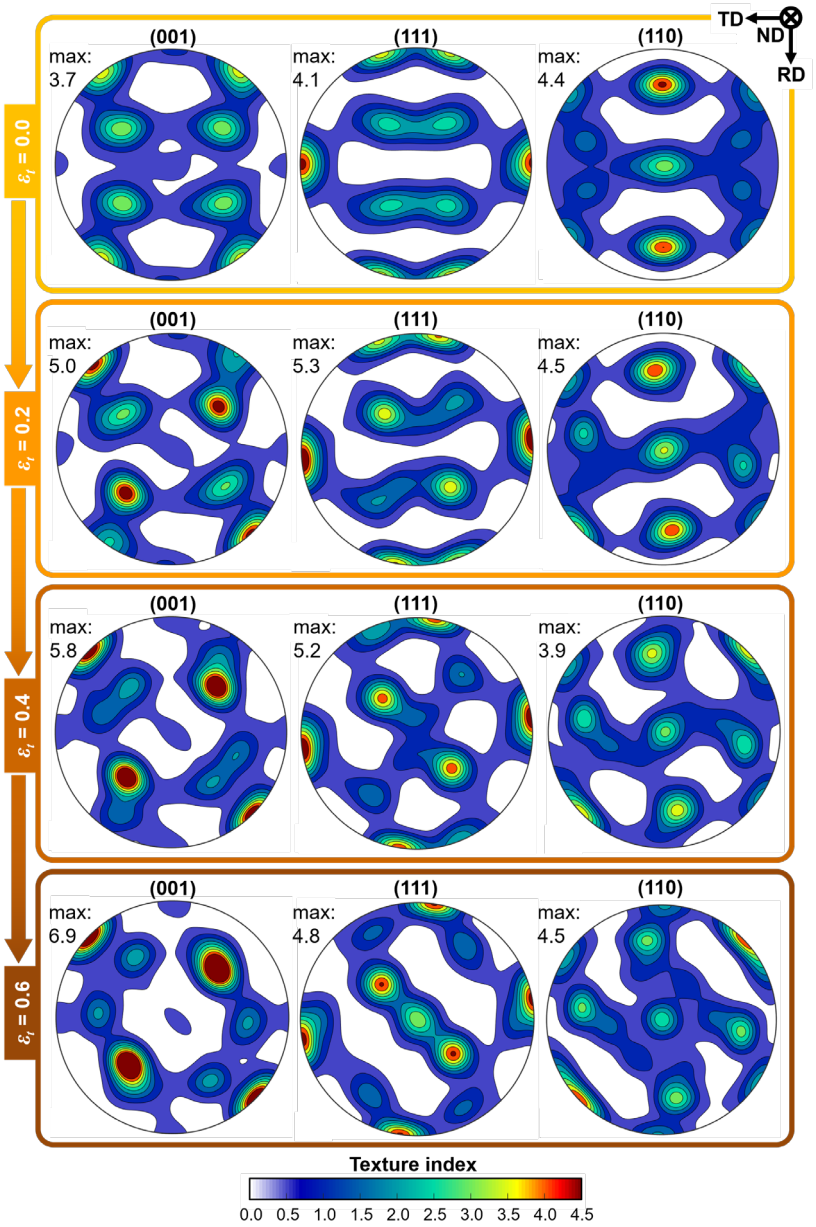

Figure 5: Evolution of pole figures of (001), (111) and (110) planes for compression in RD-TD at strains of approx. 0.0, 0.2, 0.4 and 0.6 obtained from simulation.

Tension: The original brass texture of the as-received aluminum alloy as shown in Figure 1 is more or less preserved under tension. Comparing Figure 1 with Figure 3 reveals that the predicted change of the texture during tensile deformation is negligible for each of the three directions, since only limited strain to fracture was achieved during tensile testing. The pole figures based on measurements show a slight increase of the texture index maximum in RD, RD-TD and TD, whereas VPSC modeling predicts the slight increase of the texture index maximum mainly in TD.

Compression: The original brass texture of the as-received aluminum alloy shown in Figure 1 changes considerably under compression, because as shown in Figure 2 the strain achieved during compression testing is notably higher compared to the strain achieved during tensile testing. Thus, the pole figures of the compressed samples depicted in Figure 4 differ significantly for each of the three directions RD, RD-TD and TD. Closer analysis reveals that VPSC modeling was obviously unable to predict the texture in RD, as the pole figures differ distinctly between Figure 4 (a) and (d). The measured pole figures illustrated in Figure 4 (d) form a strong but not fully developed <110> fibre texture and the texture index maximum increases significantly, whereas the calculated pole figures shown in Figure 4 (a) do not form a distinct type of texture. In contrast, VPSC modeling was

able to predict the 45°-rotated {110}<001> Goss texture with additional poles of lower intensity. The positions of the measured poles are slightly different and less symmetric; however, the overall tendency is well represented. Therefore, the area of EBSD measurement was either too small for gathering statistically relevant data, or the plastic deformation tended to form different secondary texture features in RD-TD compared to the predictions. In TD a strong {112}<11-1> copper texture was observed in both measurements and simulation. As positions and intensities of the measured and calculated poles are slightly different, crystal rotation during compression testing was virtually faster than predicted by VPSC modeling. Consideration of grain interaction and grain co-rotation to account for correlations between the orientations of neighboring grains may eventually improve the results of the performed simulation. Particularly grain co-rotation was identified by means of VPSC modeling to delay texture evolution in aluminum alloys, which tends to preserve the anisotropy at higher strains [20].

Figure 5 illustrates that with increasing deformation or strain ε_t, respectively, the texture index maximum increases and 4, 6 and 2 distinct poles form in the (001), (111) and (110) planes. The Goss texture has already formed at the strain of $\varepsilon_t \approx 0.4$, but with increasing deformation it becomes more distinct.

Summary and Conclusions

The deformation behavior of commercial rolled EN AW-7075-T651 aluminum alloy at room temperature under quasi-static tension and compression was investigated using viscoplastic self-consistent (VPSC) modeling and electron backscattered diffraction (EBSD) measurements. Flow curves and pole figures characterizing the texture of both the as-received and the deformed material were calculated and measured. The results achieved from simulation and experiments allow for drawing the following conclusions:

- In principle, VPSC modeling was successfully applied for predicting the general deformation behavior of EN AW-7075-T651 under tension and compression. However, due to the limited strain to fracture the texture evolution during tensile testing was negligible, whereas notable texture evolution during compression testing occurred.
- Typical {110}<-112> brass texture was determined for the as-delivered EN AW-7075-T651. Under tensile deformation strengthening of the brass texture was observed only in transverse direction (TD), but due to the limited strain to fracture any clear tendency was missing in rolling direction (RD) and in diagonal direction (RD-TD). Under compression the initial brass texture transformed into notable but incomplete <110> fibre texture (RD), {110}<001> Goss texture (RD-TD) and {112}<11-1> copper texture (TD), respectively.
- Under compression the difference between the initial brass texture and the deformed texture was small for a strain below $\varepsilon_t \approx 0.2$. As grain rotation within the microstructure became more pronounced at higher strain, considerable difference of the textures was observed for a strain beyond $\varepsilon_t \approx 0.4$. Therefore, considering interaction and co-rotation of neighboring grains may eventually improve the results of the simulation at higher strain.
- The applied VPSC modeling method describes slip mechanisms in single-phase microstructures and considers strain hardening according to the simple Voce law. Despite these simplifications VPSC modeling was generally feasible for predicting the flow curves and texture evolution. Differences between measurements and simulation could be attributed to the complex strain hardening behavior of the multiphase microstructure of EN AW-7075-T651.
- In the present work the tangent approach was used for calculating the macroscopic viscoplastic compliance of EN AW-7075-T651. In order to predict texture evolution in high-strength 7xxx aluminum alloys by means of VPSC modeling more accurately, identification of approaches which are more suitable for particular deformation modes and their experimental validation is an ongoing work.

Acknowledgement

This work was partly supported by the Austrian Research Promotion Agency (FFG) within the framework of the AMALFI project (FFG project number 872641), and by the Christian Doppler Research Association (CDG) within the framework of the Christian Doppler Laboratory (CDL) for Design of High-Performance Alloys by Thermomechanical Processing. The authors would like to thank Dr. Ricardo A. Lebensohn for kindly providing the VPSC 7c code.

References

[1] H. Hu, Texture of Metals, Texture 1 (1974) 233-258.
[2] H.-J. Bunge, Three-dimensional texture analysis, Int. Mater. Rev. 32 (1987) 265-291.
[3] S. Suwas, R.K. Ray, Crystallographic Texture of Materials, Springer London 2014.
[4] F. Roters, P. Eisenlohr, L. Hantcherli, D.D. Tjahjanto, T.R. Bieler, D. Raabe, Overview of constitutive laws, kinematics, homogenization and multiscale methods in crystal plasticity finite element modeling: Theory, experiments, applications, Acta Mater. 58 (2010) 1152-1211.
[5] D. Helm, A. Butz, D. Raabe, P. Gumbsch, Microstructure-based description of the deformation of metals: theory and application, JOM 63 (2011) 26-33.
[6] R.A. Lebensohn, C.N. Tomé, A Self-Consistent Anisotropic Approach for the Simulation of Plastic Deformation and Texture Development of Polycrystals: Application to Zirconium Alloys, Acta Metall. Mater. 41 (1993) 2611-2624.
[7] R.A. Lebensohn, C.N. Tomé, A self-consistent viscoplastic model: prediction of rolling textures of anisotropic polycrystals, Mater. Sci. Eng. A 175 (1994) 71-82.
[8] D. Tang, W. Fang, X. Fan, T. Zou, Z. Li, H. Wang, D. Li, Y. Peng, P. Wu, Evolution of the Material Microstructures and Mechanical Properties of AA 1100 Aluminum Alloy within a Complex Porthole Die during Extrusion, Materials 12 (2019) 16.
[9] S.-H. Choi, F. Barlat, Prediction of macroscopic anisotropy in rolled aluminum-lithium sheet, Scripta Mater. 41 (1999) 981-987.
[10] M. Suresh, A. Sharma, A.M. More, R. Kalsar, A. Bisht, N. Nayan, S. Suwas, Effect of equal channel angular pressing (ECAP) on the evolution of texture, microstructure and mechanical properties in the Al-Cu-Li alloy AA2195, J. Alloys Compd. 785 (2019) 972-983.
[11] X. Chen, Y. Peng, C. Chen, J. Li, K. Wang, T. Wang, Mechanical behavior and texture evolution of aluminum alloys subjected to strain path changes: Experiments and modeling, Mater. Sci. Eng. A. 757 (2019) 32-41.
[12] S.-H. Choi, J.C. Brem, F. Barlat, K.H. Oh, Macroscopic anisotropy in AA 5019A sheets, Acta Mater. 48 (2000) 1853-1863.
[13] S.-H. Choi, J.-K. Choi, H.-W. Kim, S.-B. Kang, Effect of reduction ratio on annealing texture and *r*-value directionality for a cold-rolled Al-5% Mg alloy, Mater. Sci. Eng. A 519 (2009) 77-87.
[14] L. Hu, A.D. Rollett, M. Iadicola, T. Foecke, S. Banovic, Constitutive Relations for AA 5754 Based on Crystal Plasticity, Metall. Mater. Trans. A 43 (2012) 854-869.
[15] M.A. Iadicola, L. Hu, A.D. Rollett, T. Foecke, Crystal plasticity analysis of constitutive behavior of 5754 aluminum sheet deformed along bi-linear strain paths, Int. J. Solids Struct. 49 (2012) 3507-3516.
[16] A. Pandey, A.S. Khan, E.-Y. Kim, S.-H. Choi, T. Gnäupel-Herold, Experimental and numerical investigations of yield surface, texture, and deformation mechanisms in AA 5754 over low to high temperatures and strain rates, Int. J. Plast. 41 (2013) 165-188.
[17] O. Engler, J. Aegerter, Texture and anisotropy in the Al-Mg alloy AA 5005 – Part II: Correlation of texture and anisotropic properties, Mater. Sci. Eng. A 618 (2014) 663-671.
[18] K. Wang, B. Zhou, J. Li, J.E. Carsley, Y. Li, Characterization of Plastic Anisotropy of AA 5182-O Sheets During Prestraining and Subsequent Annealing, J. Manuf. Sci. Eng. 140 (2018) 081004.
[19] Z. Li, Z. Zhang, G. Zhou, P. Zhao, Z. Jia, W.J. Poole, The effect of Mg and Si content on the microstructure, texture and bendability of Al-Mg-Si alloys, Mater. Sci. Eng. A 814 (2021) 141199.

[20] C.N. Tomé, R.A. Lebensohn, C.T. Necker, Mechanical Anisotropy and Grain Interaction in Recrystallized Aluminum, Metal. Mater. Trans. A 33 (2002) 2635-2648.
[21] X. Wang, M. Guo, Y. Zhang, H. Xing, Y. Li, J. Luo, J. Zhang, L. Zhuang, The dependence of microstructure, texture evolution and mechanical properties of Al-Mg-Si-Cu alloy sheet on final cold rolling deformation, J. Alloys Compd. 657 (2016) 906-916.
[22] X. Wang, M. Guo, J. Zhang, L. Zhuang, Effect of Zn addition on the microstructure, texture evolution and mechanical properties of Al-Mg-Si-Cu alloys, Mater. Sci. Eng. A 677 (2016) 522-533.
[23] O. Fergani, A. Tabei, H. Garmestani, S.Y. Liang, Prediction of polycrystalline materials texture evolution in machining via Viscoplastic Self-Consistent modeling, J. Manuf. Process. 16 (2014) 543-550.
[24] O. A. Velazquez-Carrillo, F. A. García-Pastor, Thermal stability of microstructure, mechanical properties, formability parameters and crystallographic texture in an Al-7075 alloy processed by accumulative roll bonding, J. Mater. Res. Technol. 11 (2021) 2208-2220.
[25] B. Zhou, B. Liu, S. Zhang, The Advancement of 7XXX Series Aluminum Alloys for Aircraft Structures: A Review, Metals 11 (2021) 718.
[26] D.G. Brandon, The structure of high-angle grain boundaries, Acta Metall. 14 (1966) 1479-1484.
[27] C.N. Tomé, R.A. Lebensohn, Manual for Code Viscoplastic Self-Consistent (VPSC) Version 7c, Los Alamos, 2009.
[28] R.A. Lebensohn, C.N. Tomé, P. Ponte Castañeda, Self-consistent modelling of the mechanical behaviour of viscoplastic polycrystals incorporating intragranular field fluctuations, Philos. Mag. 87 (2007) 4287-4322.
[29] C. Tomé, G.R. Canova, U.F. Kocks, N. Christodoulou, J.J. Jonas, The relation between macroscopic and microscopic strain hardening in F.C.C. polycrystals. Acta Metall. 32 (1984) 1637-1653.
[30] G.E. Dieter, Mechanical Metallurgy SI Metric Edition, 3rd ed., McGraw-Hill, London, 1988.
[31] R.F.S. Hearmon, Temperature dependence of the elastic constants of aluminium, Solid State Commun. 37 (1981) 915-918.
[32] MTEX Toolbox | MTEX, https://mtex-toolbox.github.io (accessed Nov. 29, 2021).
[33] T. Børvik, O.S. Hopperstad, K.O. Pedersen, Quasi-brittle fracture during structural impact of AA7075-T651 aluminium plates, Int. J. Impact Eng. 37 (2010) 537-551.
[34] M. Fourmeau, T. Børvik, A. Benallal, O.G. Lademo, O.S. Hopperstad, On the plastic anisotropy of an aluminium alloy and its influence on constrained multiaxial flow, Int. J. Plast. 27 (2011) 2005-2025.
[35] K. Senthil, M.A. Iqbal, P.S. Chandel, N.K. Gupta, Study of the constitutive behavior of 7075-T651 aluminum alloy, Int. J. Impact Eng. 108 (2017) 171-190.
[36] A.D. Rollett, R. Campman, D. Saylor, Three Dimensional Microstructures: Statistical Analysis of Second Phase Particles in AA7075-T651, Mater. Sci. Forum 519-521 (2006) 1-10.
[37] A. Kazemi-Navaee, R. Jamaati, H. Jamshidi Aval, Asymmetric cold rolling of AA7075 alloy: The evolution of microstructure, crystallographic texture, and mechanical properties, Mater. Sci. Eng. A 824 (2021) 141801.